frontiers | Frontiers in Earth Science

TYPE Original Research
PUBLISHED 08 March 2023
DOI 10.3389/feart.2023.1131386

OPEN ACCESS

EDITED BY
Chaojun Fan,
Liaoning Technical University, China

REVIEWED BY
Xiangjun Chen,
Henan Polytechnic University, China
Jianwei Cheng,
China University of Mining and Technology, China

*CORRESPONDENCE
Huice Jiao,
pdsjhc@163.com

SPECIALTY SECTION
This article was submitted to Economic Geology, a section of the journal Frontiers in Earth Science

RECEIVED 25 December 2022
ACCEPTED 21 February 2023
PUBLISHED 08 March 2023

CITATION
Song W, Jiao H and Wang Y (2023), Crack closure effect during the impact coal seam with high-pressure air blasting and the influence of gas drainage efficiency. *Front. Earth Sci.* 11:1131386. doi: 10.3389/feart.2023.1131386

Crack closure effect during the impact coal seam with high-pressure air blasting and the influence of gas drainage efficiency

Weihua Song[1,2], Huice Jiao[2]* and Yingwei Wang[1]

[1]State Key Laboratory of Coking Coal Exploitation and Comprehensive Utilization, China Pingmei Shenma Corporation Group, Pingdingshan, Henan, China, [2]College of Mining, Liaoning Technical University, Fuxin, Liaoning, China

The crack closure in impact coal seams induced by high-pressure air blasting greatly affects gas drainage efficiency. The length of the crack closure was calculated and analyzed based on energy and elastic theories. The closure region was then determined to be 3.8 m from the blasting hole. The results of a high-pressure air blasting experiment in the underground of one coal mine in China showed that the effect of crack closure on gas drainage efficiency manifested as a decreased amplitude of gas emission in the crack closure region. At 1.0–4.0 m from the blasting hole, the amplitude of gas emission in the observation holes first increased and then decreased with increasing distance from the blasting hole. At 1.8–2.5 m from the blasting hole, the amplitude of the gas emission was maximal. At 4.0 m from the blasting hole, the crack was nearly closed, and the gas emission in the observation holes was minimal. The theoretical calculation had good consistency with the field test results; thus, it can provide an important reference for an appropriate arrangement of gas drainage boreholes.

KEYWORDS

high-pressure air blasting, impact coal seam, gas drainage, crack closure, gas emission

1 Introduction

The coal seams in China have large amounts of coal seam gas (Dai et al., 2019; Zou et al., 2019; Huang et al., 2022; Men et al., 2022). However, the existing coal seam gas has not been sufficiently utilized due to its low permeability in the rock mass, geological complexities, and equipment limitations. The Shenyang Coal Science Research Institute pioneered the development of the compressed air blast technique and equipment that has been widely used in China (Li, 2013; Li, 2015). The application of this technique in Huainan Mine showed that the predicted influential area resulting from the compressed air blast was inconsistent with real-world data. This might be attributed to the closure of the fractures, leading to difficulties in gas transport in the rock mass. More specifically, after the compressed air is released, fractures close to the elastic rock mass zone tend to close, resulting in a reduction of the flow channels for coal seam gas transport. These fractures can only be re-opened if the high-pressure gas is pumped through into the rock mass. The present work is a case study of the influence of compressed air blasts on the performance of coal seam gas drainage.

2 Coal failure mechanism due to compressed air blasts

After the compressed air blast, the resulting blasting wave and pressure jointly damage coal through compressive and tensile stresses. The borehole wall is heavily damaged and fractured into small pieces, whereas the rock mass in the distance to the borehole wall forms fractures due to tangential stress. The fracture propagates further into the rock mass and continuously consumes energy provided by the air blast. As a result, the blasting wave-induced energy tends to decrease as it propagates further, leading to formation of only elastic failure in the rock mass (Ning, 2012; Zhang et al., 2017; Gao et al., 2018; Yang et al., 2019).

2.1 Elastic energy consumption Et due to compressed air blasts

Beyond the fracture boundary, only elastic deformation occurs due to the wave blast. The elastic deformation in the unit volume of rock δ_t is according to the following formula (Cai et al., 2014; Li et al., 2018; Cheng et al., 2022):

$$\delta_t = \frac{1}{2}(\sigma_r\varepsilon_r + \sigma_\theta\varepsilon_\theta) = \frac{{\sigma_r}^2}{2E_m}(1+\lambda^2).$$

Thus, the energy consumed due to the elastic deformation is

$$E_t = \int_{r_1}^{R_E} 2\pi r\delta_E dr,$$

$$E_t = \frac{\pi(1+\lambda^2)(p_m r_m)^2}{2E_m(\alpha-1)}\left[\left(1-\frac{r_m}{R_E}\right)^{2(1-\alpha)}\right],$$

where ε_r and ε_θ are the strain along the radial and tangential directions, respectively, relative to the borehole, m and α are coefficients where $\alpha = 2 - \nu/(1-\nu)$, $\nu = 0.3$, $\alpha = 1.57$, E_m the Young's Modulus of coal, 4.6 GPa, $r_m = b_1/2$ is the radius of the fracture, λ is a coefficient equivalent to $\nu/(1-\nu) = 0.43$, R_E is the radius at which the elastic deformation starts to occur, $R_E = \frac{1+\nu}{E_m}\frac{(\sigma_t+\sigma_w){r_m}^2}{r}$, 4.0 m, σ_t is the tensile strength, and σ_w is the initial stress.

The immediate stress induced on coal when air blasting occurs is calculated according to the following equation:

$$p_m = \frac{\rho v_p \cdot \rho_{ky}{v_s}^2}{2\left(\rho v_p + \rho_{ky} v_s\right)},$$

where ρ is the coal density (1334 kg/m^3), v_p is the compressive wave velocity (1856 m/s) determined by laboratory testing, ρ_{ky} is the density of the compressed air (83.85 kg/m^3), and v_s is the compressed air velocity at the releasing nose (243.7 m/s) as determined by measurement.

2.2 Fracture closure

After the air blast, the fracture propagates to an extent beyond which the deformation remains elastic. Once the blasting wave energy is completely consumed, the fractures at the boundary between the fracture and elastic deformation zone tend to close under the action of load F. For ease of calculation, the friction is ignored and the closure of the fractures is elastic. The energy consumption time is very short (approx. 25 μs), and the length of the coal is l (Figure 1).

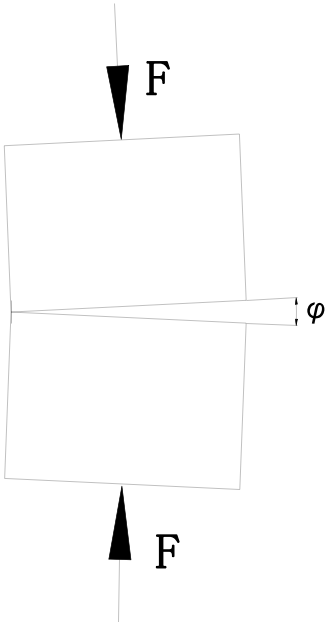

FIGURE 1
Schematic diagram of the fracture closure.

The probability of damage to the microelement of the coal is assumed to be the damage variable D according to

$$D = \int_0^J P(x)dx = 1 - \exp\left[-(J/J_0)^m\right].$$

If the rock microelement strength is J, then $\sigma_1 = \sigma_c$, $\varepsilon_1 = \varepsilon_c$ when the peak point gradient is 0, and the relevant microelement strength is J_c. When the rock at the closure zone has residual strength, $D = 1$; hence, $\exp[-(J/J_0)^m] = 0$. The strength parameters in the microelement, J, J_0, and m can be calculated as follows:

$$m = \frac{-(\sigma_c - 2\mu\sigma_3)}{(\sigma_c - 2\mu\sigma_3 - E\varepsilon_c + hE\varepsilon_c)\ln\left(\frac{\sigma_c - 2\mu\sigma_3 - E_m\varepsilon_c + \xi E_m\varepsilon_c}{hE_m\varepsilon_c}\right)},$$

$$J = \sigma_1^* + 2\sigma_3^* + \frac{\sin\varphi}{3\sqrt{3-sin^2\varphi}}(\sigma_1^* - \sigma_3^*)^2,$$

$$J_0 = J_c\left[\frac{J_1(\sigma_c - 2\mu\sigma_3 - E_m\sigma_c + \xi E_m\varepsilon_c)}{\sigma_c - 2\mu\sigma_3}\right]^{1/J_1},$$

where σ_1^* and $2\sigma_3^*$ are the effective stresses of σ_1 and σ_3, respectively, and φ is the internal friction angle.

The fracture closure coefficient ξ can be calculated according to

$$\xi = 1 - \frac{\sigma_r - 2\mu\sigma_r}{E_m\varepsilon_r},$$

where μ is the Poisson's ratio, σ_r is the residual strength in MPa, and ε_r is the residual strain.

Considering the expansion of the fracture resulting from coal seam gas adsorption in the fracture, σ_z is the summation of closure stress in coal fractures σ_e (Meng and Li, 2015; Vyacheslav et al., 2016; Peng and Zheng, 2020; Liu et al., 2022) and expansion stress σ_p, and the expansion stress due to the coal seam gas adsorption in the fractures is calculated as follows (Xue et al., 2015; Chu et al., 2022):

$$\sigma_p = \left[2aRT\rho(1-2\nu)\ln(bp)\right]\Big/(3V),$$

where a and b are adsorption coefficients, p is the compressive stress of the coal seam gas (1.2 MPa), ν is the Poisson's ratio, ρ is the coal density (334 kg/m^3), R is the molar gas constant (8.31 J/(mol·K)), T is the absolute temperature (297.35 K), and V is the molar volume (22.41 L/mol).

The effective stress σ_e and actual stress σ_Z are as follows:

$$\sigma_Z = \sigma_e + \sigma_p,$$
$$\sigma_Z = \kappa\sigma_e,$$

where κ is the effective stress coefficient according to

$$\kappa = 1 - K/K_s,$$

where K is the water bulk modulus and K_s is the coal solid particle bulk modulus. κ is 0.7.

During the blasting, the decay of the blasting wave peak in the coal mass is calculated as follows:

$$p_E = p_E\left(\frac{r_m}{r_E}\right)^3.$$

Assuming the total force on the coal in the elastic zone results only from the blasting wave,

$$p_E = F.$$

Considering the conservation of energy, the energy in the elastic zone is not completely released, with most of the energy converted to kinetic energy, while a minor portion is stored in the elastic zone.

$$E_t = E_t^1 + Q_1.$$

The simplified form is

$$E_t^{'} = \eta E_t.$$

The energy from the elastic zone is assumed to contribute to the fracture closure according to

$$E_t^{'} = \eta E_t = Fl\sin\frac{\varphi}{2}\cos\frac{\varphi}{2},$$

where η is the energy coefficient, and it equals 1 when all energy is used for fracture closure.

The length of the fracture closure is

$$1 = \frac{\frac{\eta\pi\left(1+\lambda^2\right)\left(p_m r_0\right)^2}{2E_m(\alpha-1)}\left[\left(1-\frac{r_0}{R_E}\right)^{2(1-\alpha)}\right]}{p_m\left(\frac{r_m}{r_E}\right)^3\sin\frac{\varphi}{2}\cos\frac{\varphi}{2}}.$$

The effective closure length in the fracture is

$$l_y = \xi l.$$

After compressed air blasting, fractures form, leading to an increase in the gas flow channels. In contrast, the fractures close to the elastic zone tend to close, resulting in decreased gas flow channels. Therefore, the borehole for air blasting should be drilled within the fracture propagation zone. In addition, if the borehole height is more than the height of the fracture closure zone, the amount of coal seam drainage decreases greatly.

The effective drainage zone is assumed to be as far as L from the borehole according to

$$L = a_* + b_1 + b_2 - l_y,$$

where a_* is the blasting radius (0.094 m), b_1 is the thickness of the loose area, and b_2 is the thickness of the fracture propagation.

The diameter of the loosened area can be calculated as follows (Qian, 2010):

$$b_1 = \left(\frac{(1-2\nu)(1+\nu)}{3(1-\nu)}\frac{\rho {c_p}^2}{\sigma_*}\right)^{1/3}\frac{1}{2}\frac{0.61{E_z}^{1/3}}{\left(\rho c_p\sigma_*\right)^{1/9}}.$$

The diameter of the fracture propagation is calculated as follows (Qian, 2010):

$$b_2 = \left(\frac{\rho {c_p}^2}{4\left(\frac{1+\sin\theta}{1-\sin\theta}\right)\sigma_0}\right)^{1/3}\frac{1}{2}\frac{0.61{E_z}^{1/3}}{\left(\rho c_p\sigma_*\right)^{1/9}}.$$

As such,

$$L = 0.094 + \left(\frac{(1-2\nu)(1+\nu)}{3(1-\nu)}\frac{\rho {c_p}^2}{\sigma_*}\right)^{1/3}\frac{1}{2}\frac{0.61{E_z}^{1/3}}{\left(\rho c_p\sigma_*\right)^{1/9}} + \left(\frac{\rho {c_p}^2}{4\left(\frac{1+\sin\theta}{1-\sin\theta}\right)\sigma_0}\right)^{1/3}\frac{1}{2}\frac{0.61{E_z}^{1/3}}{\left(\rho c_p\sigma_*\right)^{1/9}} - \xi\frac{\frac{\eta\pi\left(1+\lambda^2\right)\left(p_m r_0\right)^2}{2E_m(\alpha-1)}\left[\left(1-\frac{r_0}{R_E}\right)^{2(1-\alpha)}\right]}{p_m\left(\frac{r_m}{r_E}\right)^3\sin\frac{\varphi}{2}\cos\frac{\varphi}{2}},$$

where ν is Poisson's ratio (0.3), ρ is the coal density (1334 kg/m^3), and c_p is the compressive stress velocity in the coal mass (1856 m/s). η is 0.75, E_Z is the energy resulting from the blast, σ_* is the compressive strength of the coal (28.63 MPa), σ_0 is the tensile strength (0.462 MPa), $\theta = \pi/18$, and $\varphi = 2\pi/45$. Substituting all these parameters into the equation mentioned previously leads to $L = 3.8m$.

3 Field testing

3.1 Site background

The field testing was conducted in the transport roadway in a single coal mine. The compressed air blasting was initiated in a coal seam with a thickness of 3.6 m. The stress from the coal seam gas was 1.6 MPa, and the gas intake was around 6.11 m^3/t. The seam was weak and the gas permeability was 0.0111 m^2/MPa^2·d. The roadway was reinforced by cable bolts and steel mesh.

3.2 Testing methodology

A 0.5-m-deep borehole was drilled into the seam, followed by the installation of the blasting detonation. When the stress

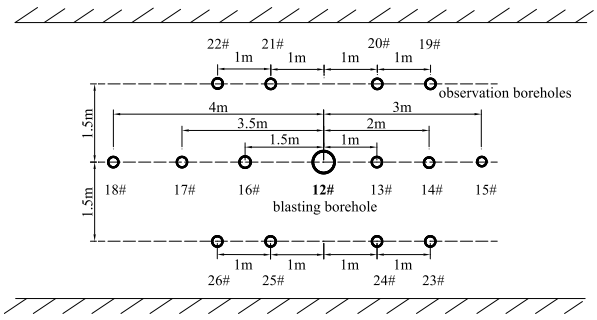

FIGURE 2
Borehole pattern.

reached 60 MPa, the compressed air was released. Two to three blasts were performed in each borehole. Eventually, one drainage borehole and 12 blasting boreholes were formed. In addition, adjacent to the blasting boreholes, another 14 boreholes were drilled for observation (Figure 2). The observation boreholes were drilled 0.5 m deep into the seam with a drill bit 94 mm in diameter. All these boreholes were sealed thereafter. Blasting boreholes were drilled similarly. As soon as the compressed air blasting occurred, the drainage borehole was connected to the gas drainage system. All gas drainage parameters were the same in each borehole. The variations in coal seam gas drainage volume during the drainage were measured. The gas drainage volumes measured in each observation borehole were used to aid in identifying the locations of fracture closure.

3.3 Testing results and analysis

As shown in Table 1 and Figure 3, blasting in 12 blasting boreholes showed increased gas flow in the observation boreholes. The observation boreholes within 2 m of the blasting holes had the largest gas flow. The gas flow decreased from the observation borehole 1 m (borehole 13) to that 1.5 m (borehole 16) from the blasting borehole. The flow then increased to the observation boreholes 1.8 m (boreholes 20, 21, 24, and 25) away from the blasting borehole before decreasing again to the observation boreholes 2 m (borehole 14) and 2.5 m (boreholes 19, 22, 23, and 26) away from the blasting borehole. The gas flow increase peaked at the observation borehole 3 m (borehole 15) from the blasting borehole and reached its minimum in the observation borehole 4 m (borehole 18) from the blasting borehole. The gas flow increase was more obvious in the zone within 3 m from the blasting borehole. The increasing rate of gas intake peaked in the zone 1.8–2.5 m from the blasting borehole. The increasing rate of gas flow peaked in the zone 1.5 m from the blasting borehole. The rate was as high as 55.56%, and the gas drainage was also enhanced most significantly in this area. The gas flow increase tended to decrease more than 2.5 m from the blasting borehole. The increasing rate reached its minimum in the zone 4 m from the blasting borehole, where it was close to the fracture closure zone.

After the air blasting, the rate of gas intake tended to increase and then decrease with distance from the blasting borehole. When approaching the fracture closure zone, the increasing rate reached its minimum. The increasing rate of the gas intake on the left-hand side of the blasting borehole was greater than that on the right-hand side. This might be attributed to the orientation of the *in situ* major

TABLE 1 Variation in coal seam gas flow before and after the compressed air blast.

Borehole no.	Before blasting		After blasting		Variation in coal seam gas flow/%
	Total gas flow/ ($mL{\cdot}min^{-1}$)	Coal seam gas volume percentage/%	Total gas flow/ ($mL{\cdot}min^{-1}$)	Coal seam gas volume percentage/%	
13	2232.55	98	3213.57	100	43.94
14	1545.87	99	2131.64	100	37.89
15	1225.61	99	1840.45	98	50.17
16	1108.60	97	1724.58	98	55.56
17	783.90	98	955.90	100	21.94
18	1382.67	98	1586.20	100	14.72
19	1487.45	97	2104.89	98	41.51
20	983.27	98	1422.99	99	44.72
21	1164.56	99	1705.73	98	46.47
22	1572.35	98	2291.81	99	45.74
23	1374.53	98	1611.08	98	17.21
24	1231.09	98	1632.79	99	32.63
25	1028.61	99	1397.06	99	35.82
26	792.54	99	923.94	98	16.58

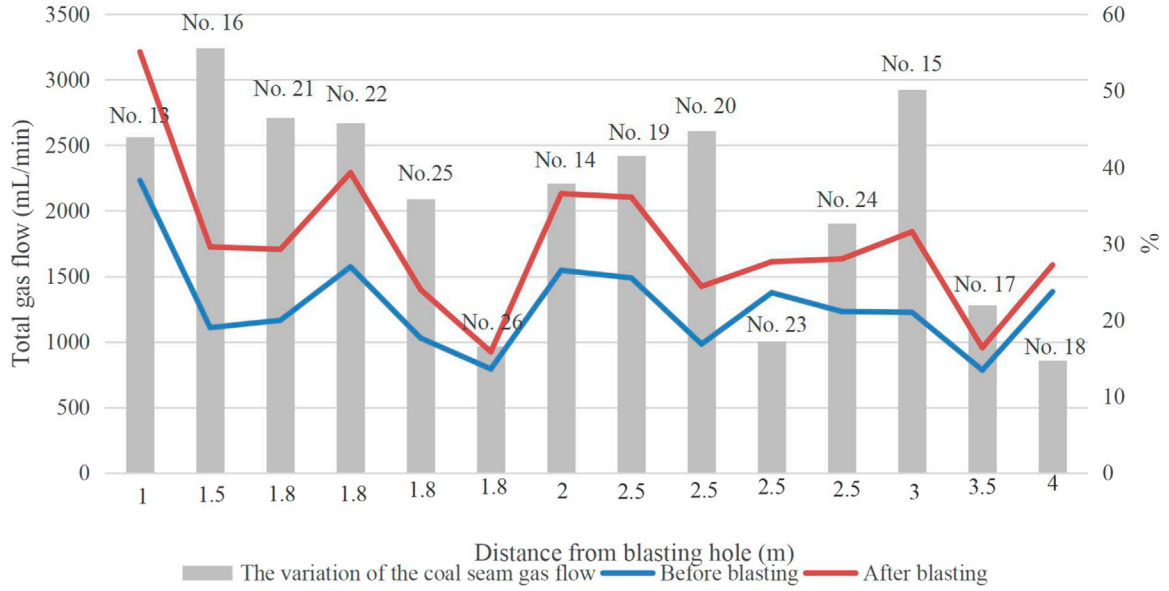

FIGURE 3
Schematic diagram of variations in coal seam gas flow.

principal stress. The observation boreholes above the blasting borehole (boreholes 19–22) had higher gas intake increase rates than those below the blasting borehole (boreholes 23–26). Although the induced stress level at the top and bottom of the blasting borehole by the blasting wave tended to be the same, the induced failure differed, with tensile and compressive failures dominating the top and bottom, respectively. As the tensile strength is always much less than the compressive strength, the influential area resulting from air blasting at the top would be much larger than that at the bottom.

4 Conclusions

a. As a result of compressed air blasting, the huge blasting wave induced extensive fractures that propagated into the coal mass, leading to increased gas flow channels. The gas intake above the air-blasting borehole was higher than that below. The difference in gas intake between the zones on the left and right was attributed to the *in situ* major principal stress.
b. The compressed air blasting propagated the fractures into the coal mass up to a certain extent, beyond which the coal mass remained intact. The fractures close to the boundary tended to close, leading to decreased gas flow channels. In other words, the real fracture length was always smaller than the theoretical fracture length.
c. The observations of gas flow and intake volumes confirmed that the fracture started closing 4 m from the blasting borehole, a finding consistent with the theoretical value of 3.8 m. This also demonstrated that the theoretical model proposed in this study could predict the fracture length and, hence, aid in coal seam gas drainage prediction. However, the gas migration in the coal seam had the characteristics of an unstable flow field and was also affected by factors such as the construction quality of the drainage hole and the gas flow in the hole. Therefore, further research is needed.

Data availability statement

The raw data supporting the conclusion of this article will be made available by the authors, without undue reservation.

Author contributions

WS wrote the main manuscript text. HJ and YW oversaw the editing of the manuscript. All authors reviewed the manuscript.

Funding

The authors declare that this study received funding from China Pingmei Shenma Corporation Group (Grant No. 41040220181107-2). The funder was not involved in the study design, collection, analysis, interpretation of data, the writing of this article, or the decision to submit it for publication. This project was supported by the Open Research Fund of State Key Laboratory of Coking Coal Exploitation and Comprehensive Utilization.

Conflict of interest

WS and YW were employed by the China Pingmei Shenma Corporation Group.

The remaining author declares that the research was conducted in the absence of any commercial or financial relationships that could be construed as a potential conflict of interest.

Publisher's note

References

Cai, F., Liu, Z. G., and Luo, Y. (2014). Propagation and attenuation characteristics of stress waves generated by explosion in high-gas coal-beds. *J. China Coal Soc.* 39 (1), 110–114. doi:10.13225/j.cnki.jccs.2013.0218

Cheng, S. F., Ye, Y., Zeng, Y. W., and Gao, R. (2022). Failure law of surrounding rock under underground explosion based on a new damage-virtual tensile crack model. *Explos. And Shock Waves* 42 (5), 055201. doi:10.11883/bzycj-2021-0414

Chu, H. B., Ren, Z. Q., Yan, S., Zhu, S. Y., Chen, Z., Ye, H. Y., et al. (2022). Experimental study on the propagation and attenuation laws of stress waves in coal under high-pressure gas impact. *J. Henan Polytech. Univ. Nat. Sci.* 9, 1–6. 1673-9787.2020100040. doi:10.16186/j.carolcarrollnki

Dai, J. X., Qin, S. F., Hu, G. Y., Ni, Y. Y., Gan, L. D., Huang, S. P., et al. (2019). Major progress in the natural gas exploration and development in the past seven decades in China. *Petroleum Explor. Dev.* 46 (06), 1100–1110. doi:10.1016/s1876-3804(19)60266-1

Gao, K., Liu, Z., and Liu, J. (2018). Propagation law and failure characteristics of blasting stress wave in structural belt coal-rock. *J. China Coal Soc.* 43, 79–86. doi:10.13225/j.cnki.jccs.2017.0798

Huang, Z. W., Li, G. F., Yang, R. Y., and Li, G. S. (2022). Review and development trends of coalbed methane exploitation technology in China. *J. China coal Soc.* 47 (9), 3212–3238. doi:10.13225./j.carolcarrollnkiJCCS.SS22.0669

Li, S. G. (2015). Key technology and equipment research and development of improving coal seam permeability by high pres`sure air blasting. *Coal Sci. Technol.* 43 (2), 92–95. doi:10.13199/j.cnki.cst.2015.02.021

Li, S. G. (2013). Numerical simulation of coal fracture caused by high-pressure air blasting. *Saf. Coal Mines* 44 (12), 163–165. doi:10.13347/j.cnki.mkaq.2013.12.053

Li, X. L., Li, Z. H., Wang, E. Y., Liang, Y. P., Niu, Y., and Li, Q. G. (2018). Spectra, energy, and fractal characteristics of blast waves. *J. Geophys. Eng.* 15 (1), 81–92. doi:10.1088/1742-2140/aa83cd

Liu, X. B., Xue, K. S., Luo, Y., Long, K., Liu, Y. N., and Liang, Z. M. (2022). The effect of pore pressure on the mechanical behavior of coal with burst tendency at a constant effective stress. *Sustainability* 14 (21), 14568. doi:10.3390/su142114568

Men, X. Y., Lou, Y., Wang, Y. B., Wang, Y. Z., and Wang, L. X. (2022). Development achievements of China's CBM industry since the 13th Five-Year Plan and suggestions. *Nat. Gas. Ind.* 42 (06), 173–178. doi:10.3787/j.issn.1000-0976.2022.06.015

Meng, Y., and Li, Z. P. (2015). Experimental study on the porosity and permeability of coal in net confining stress and its stress sensitivity. *J. China Coal Soc.* 40 (1), 154–159. doi:10.13225/j.cnki.jccs.2013.1518

Ning, J. G. (2012). *Explosion and impact dynamics*. Beijing: National Defense Industry Press.

Peng, Z., and Zheng, F. (2020). Modal properties of elastic surface waves in the presence of material anisotropy and prestress. *J. Sound Vib.* 485 (1–2), 115588. doi:10.1016/j.jsv.2020.115588

Qian, Q. H. (2010). *Impact and explosion effect in rock and soil*. Beijing: National Defense Industry Press.

Vyacheslav, N. R., Lauren, C. G., Sinisha, A. J., Yee, S., and Gino, A. I. (2016). Coal-gas interaction: Implications of changes in texture and porosity. *Int. J. Coal Sci. Technol.* 3 (1), 10–19. doi:10.1007/s40789-015-0098-6

Xue, J. H., Wang, H. P., Zhou, W., Ren, B., Duan, C., and Deng, D. (2015). Experimental research on overlying strata movement and fracture evolution in pillarless stress-reliefmining. *Int. J. Coal Sci. Technol.* 2 (1), 38–45. doi:10.1007/s40789-015-0067-0

Yang, R. S., Xu, P., and Chen, C. (2019). Interaction between blast stress waves and cracks. *Explos. And Shock Waves* 39 (8), 081102. doi:10.11883/bzycj-2018-0480

Zhang, S. C., Zhu, F. H., and Gao, K. (2017). Study on mechanism of deep-hole controlled blasting in coal seam. *China Saf. Sci. J.* 27 (9), 140–145. doi:10.16265/j.cnki.issn1003-3033.2017.09.024

Zou, C. N., Yang, Z., Huang, S. P., Ma, F., Sun, Q. P., Li, F. H., et al. (2019). Resource types, formation, distribution and prospects of coal-measure gas. *Petroleum Explor. Dev.* 46 (03), 451–462. doi:10.1016/s1876-3804(19)60026-1